ORIGINAL ARTICLE

ISSN: 0331 - 670X

https://doi.org/10.51412/psnnjp.2026.012

The Nigerian Journal of PHARMACY
AS MEN OF HONOUR WE JOIN HANDS
THE OFFICIAL ORGAN OF THE PHARMACEUTICAL SOCIETY OF NIGERIA FOUNDED 1927

Isolation, characterization, antibacterial activity and in *silico* studies of the isolated flavonol from *Indigofera welwitschii*

A. Muntaka[1,2]

[1]Department of Pharmaceutical Chemistry, Usmanu Danfodiyo University, Sokoto.
[2]Department of Pharmaceutical Chemistry, Ahmadu Bello University, Zaria

ARTICLE INFO

Article history:

Received 17 February 2026
Revised 15 April 2026
Accepted 16 April 2026
Online Published

Keywords:

Glycoside,

Indigofera welwitschii,

Phytochemical,

Quercetin

*Corresponding Author:
A. Muntaka,
Email: armuntaqa2f@yahoo.com
Tel: +234 8039684241

ABSTRACT

Background: Inflammation and skin infections pose significant health risks in both rural and urban areas, primarily due to poor hygiene, limited access to healthcare, and unsanitary conditions. Rural regions often lack medical facilities that provide timely treatment, while urban areas with high population density can worsen the spread of infections. These factors may lead to serious skin conditions that negatively affect individuals' quality of life. In Katsina State, Nigeria, the local population traditionally uses *Indigofera welwitschii* to manage skin problems related to inflammation and bacterial infections. This research objectives were to isolate, characterize, evaluate and investigate compounds for potential antihistamine and anti-inflammatory properties in an *in silico* molecular docking model against GBM EGFR from the ethyl acetate fraction of the methanol extract of the aerial parts of *Indigofera welwitschii*.
Method: This involved the use of 2.2 kg of dried and powdered plant material, which was exhaustively extracted with methanol. The resulting methanol extract was suspended in distilled water and successfully divided into different fractions: hexane (HEF), ethyl acetate (EAF), chloroform (CHF), n-butanol (NBF), and aqueous (AQF) portions. The ethyl acetate fraction, weighing 10 g, was subjected to column chromatographic separation with silica gel using a gradient elution method. This was followed by repeated gel filtration on Sephadex LH-20 and preparative thin-layer chromatography. The structures of the isolated compounds were determined using various chemical and spectroscopic methods, including 1H and 13C NMR. Among the isolated compounds, only one was obtained in high yield and evaluated for antimicrobial activity against selected dermatophytes and also through *in silico* assessment. The agar well diffusion technique was employed to assess the antibacterial activity of the isolated compound.
Results: Quercetin and a quercetin glycoside (7-O-Prenylquercetin-3'-methoxy-3-O-α-d-glucopyranoside) were identified. The bacterial inhibition observed was minimal but highest against *Escherichia coli*. Computational analysis using AutoDock Vina in PyRx yielded docking scores of -6.2, which is lower than that of the standard drugs.
Conclusion: This is the first successful extraction of these specific flavonols, accompanied by comprehensive *in silico* analyses derived from this plant species in the establishment of its ethnomedicinal claims.

INTRODUCTION

Skin infections and other skin inflammations are the most common and reported diseases in humans in the developing countries[1] and they are the common chief complaints, prompting patients to seek care in outpatient medical clinics[2]. Severe cutaneous infections can lead to tissue, organ, and nerve damage[3]. Despite advances in microbiology and the control of microorganisms, sporadic epidemics caused by pathogenic microorganisms threaten global public health[4,5,6]. In developing countries like Nigeria, where insufficient sanitation, poverty, ignorance, hunger and malnutrition, inadequate access to drugs, poor and inadequate health care systems and antibiotic resistance are major concerns, which tremendously contribute to the spread of infections and limit the benefits of the existing drugs in controlling infectious diseases. These issues call for new strategies, including the use of natural products for disease prevention and treatment[4]. Cutaneous infections affect a significant percentage of children and adults worldwide. The rise of antibiotic-resistant strains presents formidable challenges. The transmission of ringworm-causing organisms and other

pathogenic bacteria from infected animals to humans has been increasingly reported[7,8] Cellulitis, erysipelas, impetigo, folliculitis, atopic dermatitis and mycosis affect approximately 15–20% of children and 1–3% of adults globally[9]. Bacteria have the genetic ability to acquire and transmit drug resistance, as well as to emerge as multidrug-resistant strains[10,11]. Moreover, there are reports of chemicals and other toxic ingredients in orthodox preparations that destroy the epidermal layers of the skin; thus, the need for local preparations devoid of such shortcomings[12,13].

The genus *Indigofera* has been the subject of significant research, yielding over 200 identified compounds, particularly flavonoids and terpenoids, which are noted for their pharmacological activities and ethnomedicinal applications. But certain species within this genus require further investigation. like *Indigofera welwitschii* var. *welwitschii*, which remains underexplored in terms of phytochemistry and biological activities[14,47]**.** Named after botanist Friedrich Martin Welwitsch, this delicate annual shrub grows up to 40 cm tall and thrives in the rainy season[15]. Its distribution mainly spans several African countries, including Ghana, Nigeria, and Cameroon[11,16]. *I. welwitschii* contains phytochemicals with potential medicinal properties and is used in traditional medicine for managing skin infections. However, studies on phytochemical evaluation and isolation of compounds are limited. Preliminary screenings of the plant's various parts have identified compounds such as carbohydrates, glycosides, flavonoids, alkaloids, terpenoids, and saponins[47].

Figure 1: Picture of the aerial part of *Indigofera wilwitschii*

Taxanomy of *I. welwitschii*

Kingdom: Plantae
Phylum: Magnoliophyta
Division: Tracheophyta
Class: Angiosperm
Subclass: Rosids
Order: Fabales
Family: Fabaceae
Sub Family: Papilionoideae
Genus: Indigofera
Species: *Welwitschii*

METHODOLOGY

Preparation of plant materials

The aerial parts of *Indigofera welwitschii* were collected in July 2019 from Batagarawa Local Government Area in Katsina State, Nigeria. Identification was conducted at the Herbarium of the Department of Botany, Ahmadu Bello University, Zaria, by taxonomist Mallam Sanusi Namadi (voucher number ABU01702). The plant material was air-dried in shade, ground to powder, labelled, and prepared for use.

Extraction procedure

Extraction and Partitioning of Plant Material

A crude extract of 120 g was obtained after maceration and successively partitioned into five fractions: n-hexane fraction (HEF), chloroform fraction (CHF), ethyl-acetate fraction (EAF), n-butanol fraction (NBF), and a residual aqueous fraction (AQF).

Chromatographic Procedures

Thin-layer chromatographic studies (TLC)

The thin-layer chromatography (TLC) profile of the extract and its fractions was performed using pre-coated silica gel plates and an ascending technique. Manual spotting was done with a capillary tube, and samples were developed in an airtight tank at room temperature. The sample was dissolved in methanol at an approximate concentration of 20 mg/mL and spotted along a pencil line. Different solvent systems of varying polarity were used for development. Preliminary analyses employed combinations of hexane and ethyl acetate, chloroform and methanol, and chloroform and ethyl acetate. The chromatograms were visualised under daylight and UV light, followed by spraying with 10% sulfuric acid and heating at 105°C.

Column chromatographic separations of Ethylacetate fraction (EAF)

The EAF was dissolved in methanol and adsorbed onto silica gel powder, which was used to create a column for gradient elution chromatography with solvent

combinations ranging from n-hexane to methanol. A total of 110 fractions were collected and consolidated into 20 bulk fractions(A_1-A_{20}) upon TLC monitoring. Further analysis through co-TLC identified 6 major bulk fractions (B_1-B_6), with subfraction B_3 undergoing additional purification as follows to obtain the compound pure.

Purification of fraction B_3.

The bull-fraction (B_3) weighing about 400 mg was subjected to silica gel gravity column chromatography using a small column (38-inch, 4 mm in diameter).

The following chromatographic conditions were employed.

a. Elusion: isocratic

b. Stationary phase: silica gel 60-120 mesh size

c. Eluting Solvent: chloroform: methanol 5:1

d. Packing: wet packing method was used;

e. Sample loading: The sample was dissolved in a small volume of the solvent system and applied directly on top of the column.

f. Collections: 2 mL each of a total of 40 collections were made and combined based on their TLC profile to afford 4 sub-fractions B_3A_1 – B_3A_4. Fractions B_3A_2 and B_3A_3 were independently purified using gel filtration repeatedly with Sephadex LH-20, which led to the isolation of two compounds coded AM1 and AM3b, respectively, as below.

Gel filtration chromatography of B_3A_2 and B_3A_3 fractions

The gel filtration was performed using Sephadex LH-20, which was suspended in methanol and left standing to swell for 24 h before use. It was then poured into the column and allowed to set while the sample was dissolved in a small volume of the eluent (methanol) and applied to the top of the column. For subfraction B_3A_2, 2 mL each was collected, and nineteen collections were made from which fractions 7 to 14 afforded a compound coded AM1. The same procedure was adopted for fraction B_3A_3, and a total of twenty-two (22) collections were made. Their fractions were pooled together based on similarities in their TLC profiles to afford three major fractions, coded B_3A_3 (a-c). Fraction B_3A_3b was subjected to further purification using PTLC to afford a compound coded Am3b

Spectral Analysis

The two isolated compounds were taken for spectral analysis using UV, IR and NMR spectroscopic techniques to aid elucidation and propose the structure of the compounds

Antibacterial Evaluation

Preparation of Samples

Ten milligrams (10 mg) of Compound AM3b was dissolved in 1 mL of 10% (v/v) Dimethyl Sulfoxide (DMSO). This stock solution was then diluted to a concentration of 5 mg/mL.

Preparation of Media

Nutrient agar medium was prepared according to manufacturer's instructions and autoclaved at 121 ºC for 15 minutes.

Collection of Bacterial Isolates

Five clinical bacterial isolates were obtained from the microbial strain bank at the Faculty of Pharmaceutical Sciences, Usmanu Danfodiyo University, Nigeria. The isolates included three Gram-positive bacteria (*Staphylococcus aureus*, *Bacillus subtilis*, and Methicillin-resistant *Staphylococcus aureus*) and two Gram-negative bacteria (*Escherichia coli* and *Pseudomonas aeruginosa*). The organisms were stored on nutrient agar medium at 4ºC after standardization.

Standardization and Preparation of Inoculum

The organisms were collected from a 24-hour culture using sterile normal saline. The culture's turbidity was adjusted to a McFarland 0.5 standard, with an optical density of 0.10 at 625 nm, achieving a concentration of 10^6 colony-forming units per mL (cfu/mL). The standardized bacterial culture (10^6 cfu/mL) was seeded into sterile nutrient agar in 60 mm Petri dishes. Bacterial isolates were distributed in agar, and uniform wells were created using a 4.5 mm sterile cork borer. Each well was filled with 0.1 mL of sterile molten nutrient agar and 0.1 mL of extracts. A negative control with 0.1 mL of 10% DMSO and a positive control with a ciprofloxacin disc were included. Plates stood for 1 hour at room temperature for diffusion, then incubated at 37 ºC for 24 hours. Zones of inhibition were measured in mm, and the experiment was repeated in triplicate, with mean and standard deviations calculated.

Determination of Minimum Inhibitory Concentration (MIC) and Minimum Bactericidal Concentration (MBC)

The agar well diffusion as modified by Bonev and Parisot (2008)[17], and microbroth dilution was used to assess the antibacterial activity the MIC and MBC of the isolated compound (Am3b)

***In silico* studies**

Protein Crystal Structure

High-resolution, crystal structure files of the following

enzymes were obtained from RCSB Protein Data Bank (http://www.rcsb.org/pdb); PLA2 [PDB ID: 1OXR][18], H1 [PDB: 8X5Y]19.

Ligand structure preparation

The 2D structure of the compound (AM3b) was generated using Chem Draw Ultra version 12.0.2.1076 (https://www.cambridgesoft.com). These 2D structures were then converted to 3D using Spartan software. Geometrical optimization of the compounds was carried out using the PM6 semi-empirical method with Spartan, and the results were saved as mol2 files. To prepare the ligand for docking, UCSF Chimera was used to add hydrogen atoms and Gasteiger charges. The prepared ligand was also saved as a mol2 file[20].

Protein Preparation

The X-ray crystal structures of the receptors, PLA2 [PDB ID: 1OXR][18] and H1 [PDB: 8X5Y][19], were obtained from the Protein Data Bank (http://www.rcsb.org/). Before proceeding with docking, we noted the residues surrounding the co-crystallized ligands that were within a distance of less than 5 Å. We removed all crystallographic water molecules, ions, and bound ligands from the 3D structures acquired from the PDB using UCSF Chimera[21]. It is important to note that the removal of crystal water was justified, as these water molecules did not mediate the binding of the co-crystallised ligands at the active sites of their respective proteins. The co-crystallized ligands were prepared and saved as Lig.mol2, while the isolated receptors were saved as rec.pdb. The output files from Chimera were then imported into ADT[22], where we added polar hydrogens and Gasteiger charges, and subsequently saved them as pdbqt files.

Evaluation of Docking Methodologies

Before docking the test compounds, docking validation for each enzyme was performed by removing the co-crystallised ligand from the enzyme crystal structure and re-docking using the established setup parameters. The chosen method should yield a conformation that can be superimposed on the geometric conformation of the co-crystallised ligand in the active site.

Molecular Docking

The optimized molecules in pdbqt format were saved in a folder created on the desktop. The coordinates of the active sites of the ligands on the receptors were deduced using a Grid box in Autodock tool version 1.5.6. The deduced enzyme coordinates were defined in the Vina bash configuration file, as shown in Table 1.0, with a spacing of 0.375 Å. The optimized molecule was docked on each of the receptors using vina bash command on Cygwin through Virtual screening. A semi-flexible technique was adopted, whereby the receptor enzymes were kept rigid, and the ligands were flexible around the binding area of the receptor enzymes, giving different poses and binding energy. The docked complexes were visualized on the Discovery Studio visualizer to see the 2D and 3D hydrophobic interactions between the ligands and the receptors[23].

RESULTS

Isolation and Purification of Compound AM1 (Quercetin)

Gel filtration Chromatography (Sephadex LH-20) of B_3A_2

Repeated gel filtration chromatography of fraction $\mathbf{B_3A_2}$ obtained from fraction $\mathbf{B_3}$ of the ethylacetate fraction (Table 2); 2 mL was collected each and nineteen collections. Collections 7 to 14 appear as a single spot and coded compound Am1.

Table 1: Pooled column collections from purification of fraction B_3 using silica gel

S/N	No of Eluates (B_3)	Code
1	1 – 11	B_3A_1
2	12 – 19	$\mathbf{B_3A_2}$
3	20 to 37	$\mathbf{B_3A_3}$
4	38 – 40	B_3A_4

Table 2: Column collections from gel filtration of fraction B_3A_2

S/No	No of Eluates (B_3A_2)	Code
1	1 – 6	B_3A_{2A}
2	7 – 14	**B_3A_{2B} (AM1)**
3	15 – 19	B_3A_{2C}

TLC and physicochemical assessment of compound AM1

Compound AM1 exhibited a single homogeneous spot on thin-layer chromatography (TLC) (refer to Plate I) when analysed using a solvent system consisting of Chloroform and Methanol in a 5:1 ratio. The chromatogram was viewed under natural daylight and subsequently treated with a 10% sulfuric acid solution, resulting in an R_f value of 0.66 (as detailed in Table 3). The compound was observed as a deep yellow amorphous powder that demonstrated partial solubility in ethyl acetate and complete solubility in both acetone and methanol. Additionally, the compound yielded positive results in both the ferric chloride test and the Shinoda test.

Plate I: TLC chromatogram of the isolated Compound chloroform: Methanol 4:1 solvent syste

Table 3: R_f value and solubility of Am1

Solvent System	No of Spots	R_f Value	solubility
CHL: ME 5:1	1	0.66	Acetone, Methanol

Key: CHL = Chloroform, MeOH= Methanol

Table 4: 1D and 2D NMR spectral data summary for quercetin

Position	δ_H (*J* in Hz)	^{13}C-NMR	^{1}H-^{1}H-COSY	HMBC	NEOSY
2	-	148.9	-	-	-
3	-	137.4	-	-	-
4	-	177.5	-	-	-
5	-	162.6	-	-	-
6	6.07 (1H, *d*, 1.28)	94.6	H-8	C5, C7, C8,	H-8
7	-	165.8	-	-	-
8	6.28 (1H, *d*, 2.08)	99.4	H-6	C6, C9, C10	H-6
9	-	158.4	-	-	-
10	-	104.6	-	-	-
1′	-	121.8	-	-	-
2′	7.62 (1H, *d*, 2.16)	116.1	-	C2, C2′, C3′	H-3′, H-6′
3′	-	146.4	-	-	-
4′	-	148.1	-	-	-
5′	6.78 (1H, *d*, 8.48)	116.3	H-5′, H-6′	C1′, C2′, C3′	H-2′, H-6′
6′	7.53 (1H, *dd*, 2.16, 8.42)	124.3	H-5′	C1′, C2′	H-2′, H-3′

Table 5: ^{1}H and ^{13}C-NMR data of compound quercetin compared with reported literature[25]

Position	δ$_H$ (*J* in Hz)	δ$_H$ (*J* in Hz)[25]	^{13}C-NMR	^{13}C-NMR[25]
2			148.9	146.7
3			137.4	135.8
4			177.5	176.0
5			165.8	161.1
6	6.07 (1H, *d*, 1.28)	6.21 (1H, d, *J*=1.56)	104.6	97.9
7			162.6	164.2
8	6.28 (1H, *d*, 2.08)	6.42 (1H, d, *J*=1.50)	94.6	93.1
9			158.4	156.9
10			99.4	103.1
1′			121.8	122.8
2′	7.62 (1H, *d*, 2.16)	7.76 (1H, d, *J*=1.38)	124.3	114.6
3′			146.4	144.8
4′			148.1	147.7
5′	6.78 (1H, *d*, 8.48)	6.92(1H, d, *J*=8.4)	116.1	114.9
6′	7.53 (1H, *dd*, 2.16, 8.48)	7.67 (1H, dd, *J*=8.4, 1.7)	124.3	120.3

Abubakar *et al.* [25]= CD_3OD; 600 MHz

Compound AM1= CD_3OD; 400 MHz

Discussion

AM1 appeared as a yellow amorphous powder. On the TLC, compound AM1 was found to be active under UV lamp 254 and 365 nm and became yellow after spraying with 10% H2SO4. The compound tested positive to ferric chloride and shinoda reagents, suggesting the presence of phenolic and flavonoidal nucleus (Silva *et al*., 1998). The 1H NMR spectrum showed five aromatic proton signals at δ_H 7.53 (1H, *dd*, *J* = 2.16, 8.48 Hz, H-2′), δ_H 7.62 (1H, *d*, *J* = 2.16 Hz, H-6′), δ_H 6.78 (1H, *d*, *J* = 8.48 Hz, H-5′), δ_H 6.28 (1H, *d*, *J* = 2.08 Hz, H-8), δ_H 6.07 (1H, *d*, *J* = 2.08 Hz, H-6). The proton signals at δ_H 6.28 (1H, *d*, *J* = 2.08 Hz, H-8) and δ_H 6.07 (1H, *d*, *J* =2.08 Hz, H-6) revealed the presence of an AX system of 1,2,3,5-tetrasubstituted benzene ring A for flavonoidal nucleus while presence of an ABX system of 1,3,4-trisubstituted benzene ring B was observed via the protons δ_H 7.53 (1H, *dd*, *J* = 2.16, 8.48 Hz, H-2′), δ_H 7.62 (1H, d, *J* = 2.16 Hz, H-6′) and δ_H 6.78 (1H, d, J = 8.48 Hz, H-5′). These proton chemical shift values correspond to the values reported for quercetin by [24,25]. The 13C-NMR spectrum indicates a total of 15 carbon signals, including a carbonyl and aromatic carbon signals, which were assigned to their respective protons based on the results of the HSQC experiment. The carbonyl downfield signal at δ_c 177.5 ppm is characteristic of ketones and the chromone ring of established quercetin. In the COSY spectrum, the cross peaks between δ_H (6.78 and 7.62); δ_H (6.07 and 6.28) confirm their assignment to adjacent carbon atoms, while the correct assignment of the protons and carbons linkages in the molecule was confirmed through the cross peaks of J2 and J3 correlations detected on the HMBC spectroscopy, which facilitate the attachment of the rings. The compound was proposed to be 3, 5, 7, 3', 4'-pentahydroxylflavonol (Quercetin). (Figure 2). The isolation of this compound has been reported in the methanol extract of the roots, stems and leaves of various species of *Indigofera* spacies such as *I. barberi*[26], *I. aspalathoides*[27] and in *I. secundiflora* aerial parts[28]

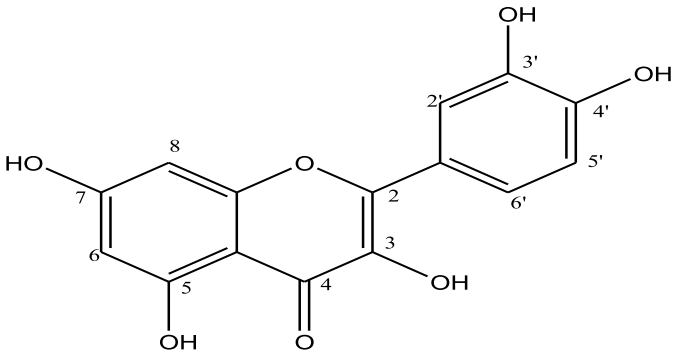

Figure 2: 3, 5, 7, 3', 4'-pentahydroxylflavonol (Quercetin)

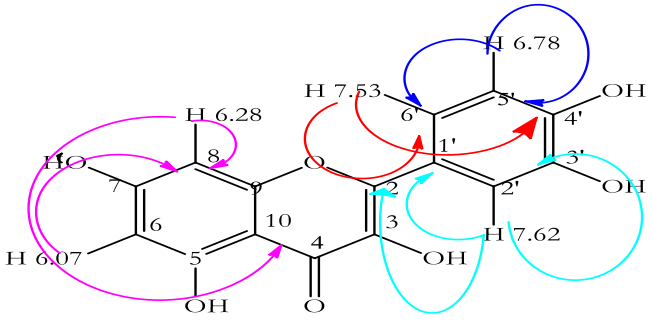

Figure 3: Major observed HMBC correlation

Isolation and Characterization of Compound AM3b

Repeated gel filtration chromatography of sub-fraction B_3A_2 obtained from the purification of fraction B_3 afforded 22 fractions and which are labeled B_3A_{3A} - B_3A_{3D}; PTLC of fraction B_3A_{2C} afforded compound AM3b (Table 6)

Table 6: Column collection of fraction B_3A_3 using gel filtration

S/No	No of Eluates (B_3A_3)	Code
1	1 – 8	B_3A_{3A}
2	9 – 14	B_3A_{3B}
3	15 – 19	**B_3A_{3C} (PTLC)**
4	20 – 22	B_3A_{3D}

TLC Profile and physicochemical properties of compound AM3b

Compound AM3b gave a single homogenous spot on TLC using two different solvent systems, i.e. chloroform: methanol (4:1) and hexane: ethylacetate (1:3) (Plate II). The compound appeared as an intense yellow amorphous powder, and it was completely soluble in methanol.

Table 7: R_f values of compound Am3b

Solvent System	No of Spots	R_f Value
CHL: MeOH 4:1	1	0.71
HEX: EA 1:3	1	0.46

Key: CHL = Chloroform, MeOH = Methanol
HEX = Hexane, EA = Ethylacetate

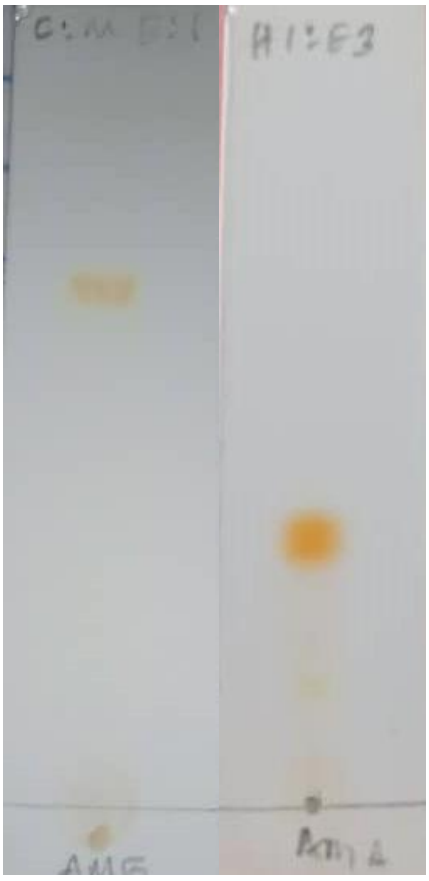

Plate II: TLC Chromatogram of the isolated compound using chloroform: Methanol 4:1 and Hexane: ethylacetate 1:3

Table 8:1D and 2D NMR spectral data summary of the compound

S/N	^{1}H-NMR	^{13}C-NMR	^{1}H-^{1}H-COSY	HMBC
2	-	157.03	-	-
3	-	133.86	-	-
4	-	177.99	-	-
5	-	161.66	-	-
6	6.19 (1H, *d,*1.51)	98.28	H-8	C-10
7	-	164.53	-	-
8	6.38 (1H, *d,*1.51)	93.28	H-6	-
9	-	157.03	-	-
10	-	104.34	-	-
1'	-	122.36	-	-
2'	7.92 (1H, s)	112.90	H-6', H-6""	C-1', C-3', C-4'
3'	-	146.95	-	-
4'	-	149.39	-	-
5'	6.90 (1H, *d*, 8.0)	114.56	H-6'	C-3', C-6'
6'	7.60 (1H, *d*, 8.0)	121.6	H-2', H-5'	C-4'
1"	5.41 (1H, d, 4.0)	102.13	H-3"	-
2"	3.55 (2H, m)	74.48	-	-
3"	3.47 (2H, m)	76.62	H-1", H-2", H-5"	C-5"
4"	3.45 (2H, m)	74.28	-	-
5"	3.29 (2H, m)	77.11	H-3"	-
6"	3.71, 3.52 (2H, m)	61.07	-	C-5"
1"'	4.29 (2H, *t*, 8.0)	66.00	-	-
2"'	2.76 (2H, s)	30.28	-	-
3"'	5.25 (1H, *d*, 4.0)	128.44	-	-
4"'	-	130.93	-	-
5"'	1.27 (3H, s)	29.34	H-6"'	C-2"', C-5"'
6"'	1.12 (3H, s)	18.83	H-5"'	C-1"'
OCH_3	3.92 (3H, s)	55.32	H-2'	C-3'

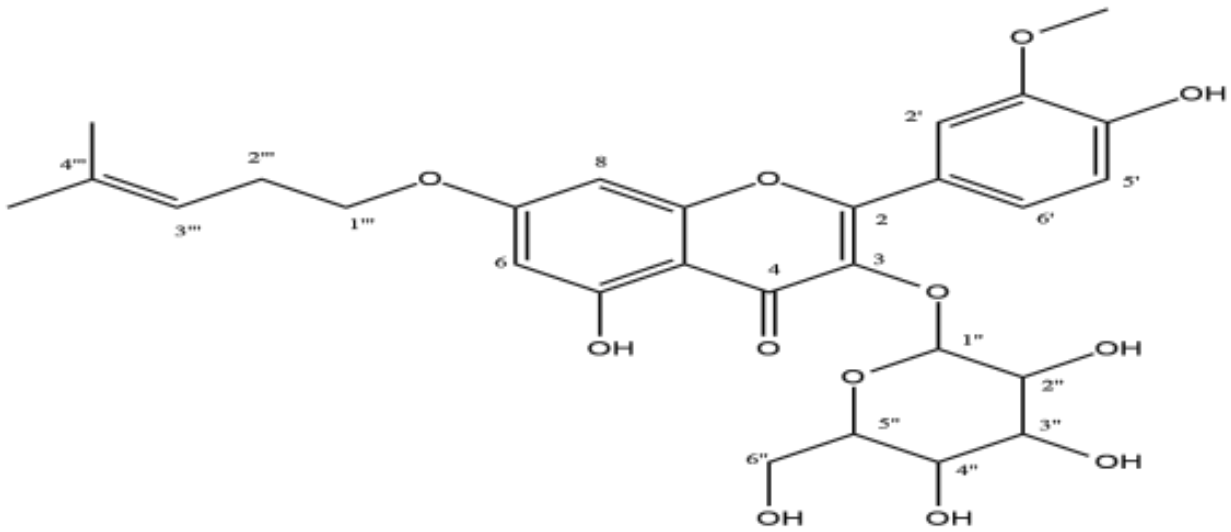

(7-O-Prenylquercetin-3'-methoxy-3-O-α-d-glucopyranoside)

Figure 4: Quercetin glycoside

Table 9: Antibacterial susceptibility test

Test organisms	Diameter zones of inhibition (Mean ± SD) (mm) 10 mg/mL	Concentration (mg/mL) MIC/MBC
SA	10.33±0.58	-
BS	11.23±0.53	-
PA	10.33±0.58	-
EC	13.33±0.58	-
MRSA	12.30±0.50	-
CPF (50 µg)	20.00 ± 0.00	
DMSO (10 %v/v)	00.00 ± 0.00	00.00 ± 0.00

Key: **SA**= *Staphylococcus aureus*; **PA**= *Pseudomonas aeruginosa*; **EC**= *Escherichia coli*; **BS**= *Bacillus subtilis*; **CPF**= Ciprofloxacin; **DMSO**= Dimethyl sulphoxide **MRSA**= Methicillin-resistant *Staphylococcus aureus;* **MIC**: Minimum Inhibitory Concentration; **MBC**: Minimum Bactericidal Concentration

Table 10: *In silico* studies

Binding affinity and molecular interactions of two anti-inflammatory target proteins with a novel Quercetin glucopyranose derivative and their respective native ligands, as obtained from PDB			
PDB ID	Ligands	Estimated free energy of binding (Kcal/mol)	Residues involved in bonded interactions and the type of interactions
1OXR (PLA2)	Quercetin glycoside (Isolated)	-6.2	LYS31: Conventional Hydrogen Bond; TYR64: Conventional Hydrogen Bond; GLY30: Conventional Hydrogen Bond; GLY30: Carbon Hydrogen Bond; PHE22: Carbon Hydrogen Bond; PHE5: Pi-Pi Stacked; TRP19: Pi-Pi T-shaped; LEU2: Alkyl; TYR64: Pi-Alkyl; PHE65: Pi-Alkyl; LEU2: Pi-Alkyl; LEU2: Pi-Alkyl; ALA23: Pi-Alkyl
	Aspirin (AIN)	-6.6	TYR64: Conventional Hydrogen Bond; TYR28: Conventional Hydrogen Bond; ASP49: Conventional Hydrogen Bond; PHE5: Pi-Pi T-shaped;
8X5Y (H1)	Quercetin glycoside (Isolated)		ASN84:Conventional Hydrogen Bond; TYR108:Conventional Hydrogen Bond; THR182:Conventional Hydrogen Bond; HIS450:Conventional Hydrogen Bond; TYR458:Conventional Hydrogen Bond; GLU181: Conventional Hydrogen Bond; H67: Conventional Hydrogen Bond; CYS180: Carbon Hydrogen Bond; ASP107: Pi-Anion; TYR108: Pi-Donor Hydrogen Bond; H71: Pi-Donor Hydrogen Bond; TRP428: Pi-Sigma; TYR108: Pi-Pi T-shaped; TYR431: Pi-Pi T-shaped; ILE115: Alkyl; PHE199: Pi-Alkyl; PHE199: Pi-Alkyl; PHE424: Pi-Alkyl; TRP428: Pi-Alkyl; PHE432: Pi-Alkyl; ILE454: Pi-Alkyl
	Astemizole (XB7)	-12.2	TYR431: Conventional Hydrogen Bond; TYR458: Carbon Hydrogen Bond; TRP158: Pi-Pi T-shaped; TRP428: Pi-Pi T-shaped; PHE432: Pi-Pi T-shaped; PHE435: Pi-Pi T-shaped; TYR108: Pi-Pi T-shaped; PHE432: Pi-Pi T-shaped; LEU88: Alkyl; MET451: Alkyl; TYR87: Pi-Alkyl;

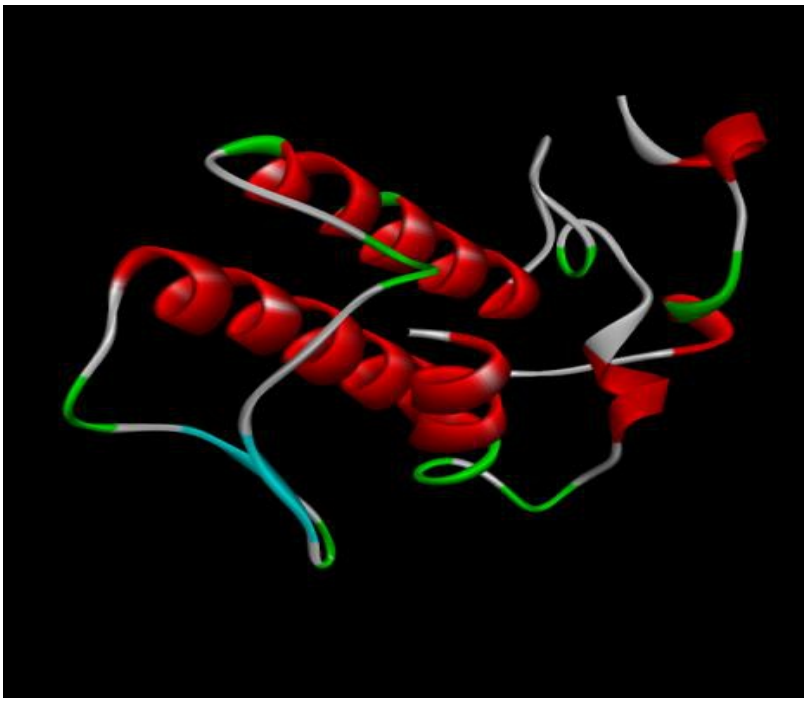

Figure 5.0: 3D structures of modeled PLA_2

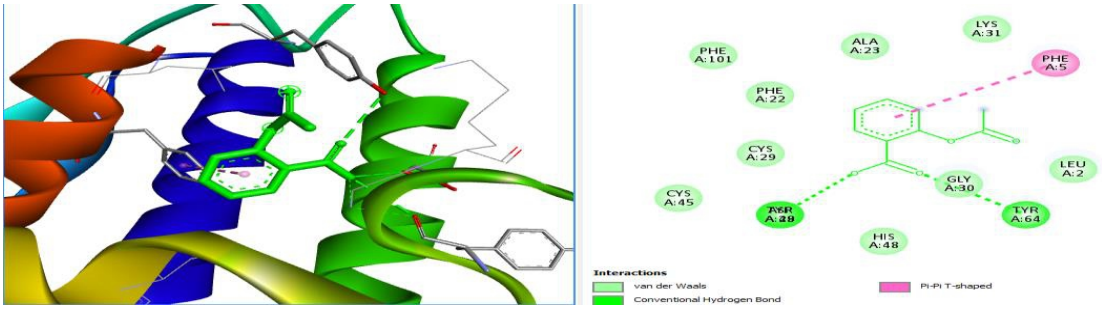

Figure 6.0: Interaction of native ligand with receptor (PLA2)

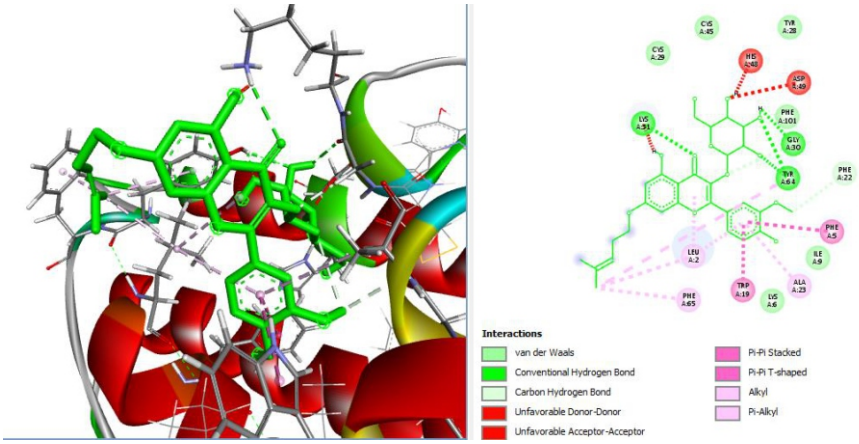

Figure 7.0: Interaction of quercetin glucopyranose with amino

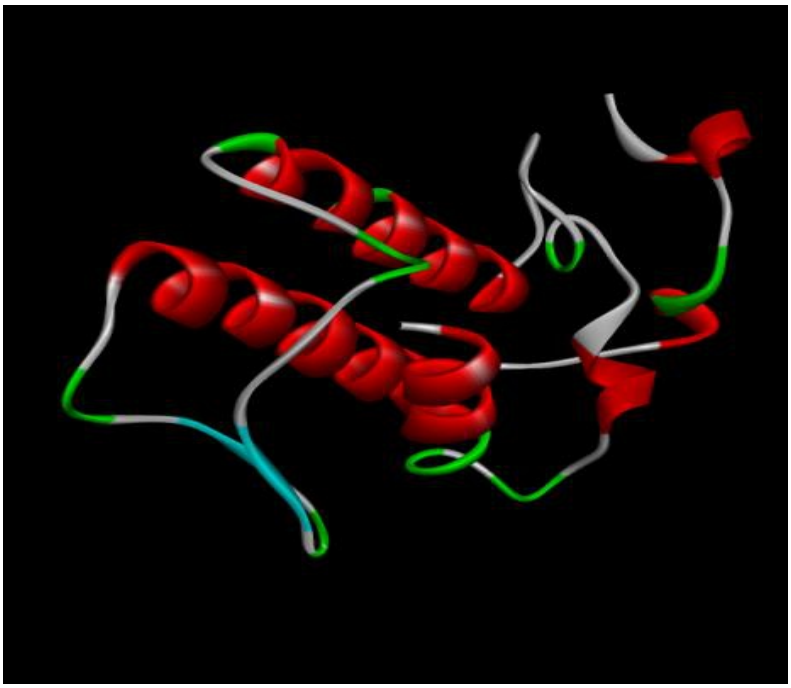

Figure 8: Dock Validation of H1 with Native Ligand (ASTEMIZOLE)

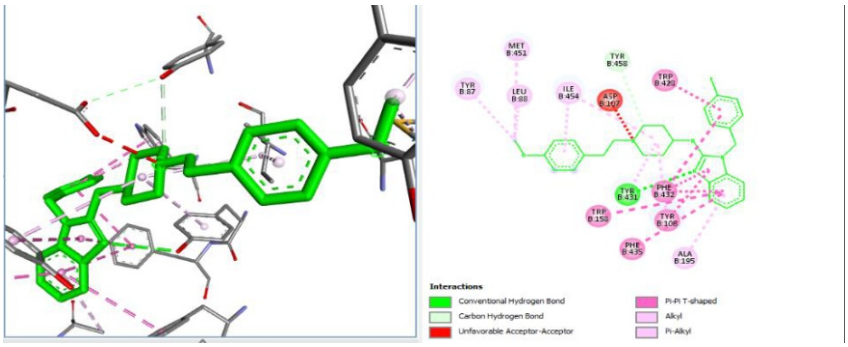

Figure 9.0: Interaction of native ligand with receptor (H1)

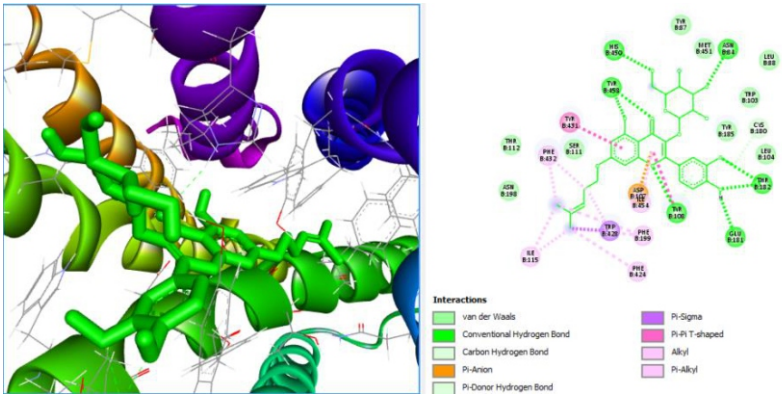

Figure 10.0: Interaction of quercetin glucopyranose with amino residues in the active site of H1

Discussion

The Compound (AM3b) was obtained as an intense yellow amorphous powder completely soluble in methanol, and it gave positive results to ferric chloride and shinoda reagent, suggesting the presence of a phenolic nucleus[29]. The IR data of compound AM3b indicated functional groups which include vibrations of the hydroxyl group, C-H stretching, carbonyl functional group, C=C olefin ring, asymmetric C-O-C stretching, and substituted benzene at (OH 3347 cm^{-1}, C=O 1740 cm^{-1}, C=C 1654 cm^{-1} Ar 1606 cm^{-1} and 820 cm^{-1}), respectively. ^{1}H-NMR spectrum revealed two doublets at δ_H 6.19 (*d,* 1.51) and 6.38 (*d,* 1.51) which were assigned to 1,2,3,5-tetrasubstituted benzene ring A while the presence of a 1.3,4-trisubstituted benzene ring B was observed by the presence of a pair of ortho-coupled protons at δ_H 7.60 (1H, *d*, *J*=8.0 Hz, 6') and δ_H 6.60 (1H, *d*, *J*=8.0 Hz, 5') alongside a singlet at δ_H 7.92 (1H, *s*, 2'), typical of flavonoids[25,30]. The sugar moiety was defined by the presence of an anomeric proton at δ_H 5.41 (1H, *d*, *J*=4.0, H-1") alongside other resonances ranging from 3.29 – 3.71 ppm, typical of glucopyranoside sugar[31,32]. Additional peaks at δ_H4.29 (2H, *t*, 8.0), 2.76 (2H, s), 5.25 (1H, *d*, 4.0), 1.27 (3H, s), 1.12 (3H, s), 3.92 (3H, s), typical of isoprenyl side chain[25,33].

The ^{13}C-NMR (125 MHz, CD_3OD) and DEPT experiments of compound AM3b revealed the presence of twenty-nine carbon atoms, which consist of eleven quaternary (C), eleven methine (CH), two methylene (CH_2) and three methyl (CH_3) carbon atoms (Table 8). The downfield signal, which resonated at δ_C 177.99 was due to a carbonyl group, and the presence of a resonance at δ_C 133.86 suggests a flavonol-type nucleus[34]. Aliphatic resonances observed at *δc* 66.00, 30.28, 128.44, 130.93, 29.34 and 18.83 further confirmed the presence of an isoprenyl chain within the molecule.

^{1}H-^{1}H-COSY experiment of AM3b revealed the protons that are situated in the same environment; placement of protons on the 1,2,3,5-tetrasubstituted benzene ring A was confirmed via cross peaks observed between H-6 and H-8. The correct assignment of .3,4-trisubstituted benzene ring B was confirmed via the cross peaks observed between the protons at H-2', H-5' and H-6'. Correlation of H-6' and H-6"" confirmed the attachment of the methoxy group on position C-3' of ring B, among others (Table 8). HSQC spectrum of AM3b assisted in assigning all protons to their respective carbons (Table 8). The HMBC spectrum of AM3b was used to establish the connectivity between the protons, carbons and the various sub-structures in the molecule. Long range correlation observed between H-2' and C-1', C-3', C-4', H-5' and C-3', C-6' and H-6' and C-3', C-6' confirmed the correct assignment of ring B while the correlation of H-6 to C-10 confirmed the assignment of ring A. Major correlations observed within the isoprenyl moiety were between H-5'" and C-2'", C-5'" and H-6'" and C-1'" and the correct assignment of the methoxy group on the ring B was observed via the correlation of 3.92 (H-6"") and C-3'. The attachment of the prenyl chain was confirmed via the higher chemical shift value observed at C-7 (164.53)[25,33,35]. Based on the 1D and 2D-NMR spectral data (Table 8). The structure of compound AM3b (Figure 4) was proposed to be 7-O-Prenylquercetin-3'-methoxy-3-O-α-d-glucopyranoside. The isolation of this compound has been reported in other spacies of the Indigofera genus such as in *I. caerulea* fruits[36], *I. tinctoria* leaves[37], *I. hartwegii*[38], *I. suffruticosa* leaves[39] and *I. aspalathoides*[27]

The observed interaction profile of quercetin glycoside within the active site PLA_2 suggests a mechanistically distinct and potentially more versatile mode of enzyme inhibition compared to aspirin. PLA_2 is a key enzyme in the inflammatory cascade, catalysing the hydrolysis of membrane phospholipids to release arachidonic acid, the precursor for prostaglandin and leukotriene synthesis[40]. Therefore, differences in ligand to residue interactions within its binding site have important implications for anti-inflammatory drug design.

Aspirin, as the native ligand, demonstrates a relatively focused binding pattern characterized by conventional hydrogen bonding with residues such as TYR64, TYR28, and ASP49, alongside a π–π T-shaped interaction with PHE5. These interactions are consistent with the role of hydrogen bonding in stabilizing ligand positioning and facilitating electrostatic complementarity within enzyme active sites[41]. The involvement of ASP49 is particularly significant, as this residue is part of the catalytic network of PLA_2 and plays a crucial role in calcium-mediated catalysis[42]. Consequently, aspirin's interaction with these residues supports its known anti-inflammatory activity through indirect suppression of arachidonic acid metabolism.

In contrast, quercetin glycoside exhibits a broader and more complex interaction network, involving multiple hydrogen bonds (LYS31, TYR64, and GLY30) and diverse π-based interactions with aromatic residues such as PHE5, TRP19, and TYR64. The shared involvement of TYR64 in both ligands underscores its importance as a stabilizing anchor within the binding pocket. However, the additional hydrogen bonds formed by quercetin glycoside suggest enhanced binding specificity and affinity, which are critical determinants of inhibitory potency[43]. The engagement of GLY30 and LYS31, residues not utilized by aspirin, further indicates that quercetin glycoside may access slightly different spatial regions within the binding site, potentially leading to altered conformational effects on the enzyme.

The prominence of π–π stacked and T-shaped interactions with residues such as PHE5 and TRP19 highlights the importance of aromatic interactions in ligand stabilization and orientation. These interactions are known to significantly contribute to binding free energy, particularly in protein pockets enriched with aromatic amino acids[44]. Additionally, the presence of π–alkyl interactions involving LEU2, TYR64, and PHE65 reflects substantial hydrophobic engagement, suggesting that quercetin glycoside effectively occupies nonpolar regions of the active site. Such hydrophobic contacts are often associated with increased ligand residence time and improved inhibitory efficiency[43].

Importantly, the interaction of quercetin glycoside with residues such as TRP19, LEU2, and GLY30 which is absent in aspirin binding, suggest a broader binding affinity and possibly a multi-site or allosteric influence on enzyme function. This expanded interaction profile may translate into enhanced inhibition of PLA_2 activity, potentially through both competitive and non-competitive mechanisms. From a pharmacological perspective, this could result in improved efficacy or reduced off-target effects, as ligands with diversified binding modes are often less susceptible to resistance or enzymatic adaptation[41].

Therefore, these findings suggest that quercetin glycoside possesses a structurally and functionally richer interaction pattern within the PLA_2 active site compared to aspirin. This not only reinforces its potential as a potent natural anti-inflammatory agent but also highlights its value as a lead scaffold for the development of novel PLA_2 inhibitors with improved specificity and therapeutic profiles.

The interaction profile of astemizole with the histamine H1 receptor reflects a well-defined and highly optimized binding mode typical of first-generation H1 antagonists. The H1 receptor, a G-protein-coupled receptor (GPCR), plays a central role in mediating allergic and inflammatory responses through histamine signaling; thus, its inhibition is a validated therapeutic strategy in allergy and inflammation management[45]. The binding interactions observed for astemizole therefore provide an important reference framework for evaluating the pharmacological relevance of quercetin glycoside.

Astemizole demonstrates a relatively structured interaction network dominated by a key conventional hydrogen bond with TYR431 and a weaker carbon hydrogen bond with TYR458. Hydrogen bonding is critical for ligand anchoring and specificity in GPCR–ligand interactions, particularly within conserved residues that stabilize the ligand in the ականի site[48]. The involvement of TYR431 suggests that this residue may serve as a primary anchoring point, while TYR458 contributes secondary stabilization. In addition to these polar interactions, astemizole forms multiple π–π T-shaped interactions with aromatic residues such as TRP158, TRP428, PHE432, PHE435, and TYR108. These interactions are characteristic of ligands targeting GPCR binding pockets, which are often rely on π-stacking to maintain ligand orientation and binding affinity[46]. Furthermore, alkyl and π–alkyl interactions with residues such as LEU88, MET451, and TYR87 highlight the importance of hydrophobic contacts in reinforcing ligand residence within nonpolar regions of the receptor.

In comparison, quercetin glycoside exhibits a markedly broader and more intricate interaction network, suggesting a potentially enhanced binding affinity and alternative inhibitory behavior. The formation of multiple conventional hydrogen bonds with residues including ASN84, TYR108, THR182, HIS450, TYR458, GLU181, and HIS67 indicates a highly stabilized ligand–receptor complex. The shared involvement of TYR108 and TYR458 between quercetin glycoside and astemizole implies partial overlap in binding orientation, reinforcing the importance of these residues in ligand recognition and stabilization. The presence of π–π interactions with TYR108 and TYR431, similar to astemizole, indicates that quercetin glycoside retains key aromatic contacts necessary for proper ligand positioning. Notably, the additional π–sigma interaction with TRP428 introduces another layer of stabilization, which may contribute to improved binding efficiency. Aromatic and π-based interactions are known to significantly influence ligand affinity in GPCR systems, often complementing hydrogen bonding by stabilizing ligand conformation within hydrophobic cavities[44]. Moreover, the identification of a π–anion interaction with ASP107 represents a distinctive feature of quercetin glycoside binding.

Hydrophobic interactions further differentiate the binding profiles of the two ligands. While both compounds engage hydrophobic residues, quercetin glycoside demonstrates a more extensive network of π–alkyl interactions involving ILE115, PHE199, PHE424, TRP428, PHE432, and ILE454. This expanded hydrophobic engagement suggests that quercetin glycoside more effectively occupies the receptor's nonpolar pockets, which can increase binding stability and prolong ligand residence time, an important determinant of pharmacological efficacy[43]. The shared interaction with PHE432 further supports the notion of partial structural similarity in binding modes, while the additional residues uniquely engaged by quercetin glycoside indicate a broader binding footprint.

Therefore, the comparative binding analysis highlights that while astemizole exhibits a classic and efficient GPCR-

binding profile, quercetin glycoside demonstrates a more versatile interaction network within the H1 receptor. This expanded binding repertoire not only underscores its potential as a natural H1 antagonist but also positions it as a promising lead compound for the development of novel anti-inflammatory agents with improved efficacy and possibly better safety profile

Relevance to Anti-Inflammatory Research

Quercetin glycoside has a wide-ranging interaction profile with the H1 receptor, indicating its potential as a novel anti-inflammatory compound. Its capability to interact with key residues such as TYR108, TYR431, TRP428, and PHE432 many of which are also involved in astemizole binding suggests that quercetin glycoside may function as a competitive inhibitor of histamine during inflammatory responses.

Additionally, quercetin glycoside displays further interactions, including a Pi-anion interaction with ASP107 and hydrogen bonds with HIS450 and GLU181. These interactions suggest that quercetin glycoside could offer stronger or more sustained inhibition of the H1 receptor compared to astemizole. This broad interaction profile indicates that quercetin glycoside could be further optimized to enhance its anti-inflammatory activity.

CONCLUSION

Two compounds, quercetin and a prenylated quercetin glycoside, were isolated from the phytoconstituents of the EAF and identified through NMR spectroscopy. the prenylated quercetin glycoside was evaluated for antibacterial activity, with in silico studies revealing that the quercetin glycoside forms seven hydrogen bonds with the H1 receptor, compared to two for astemizole. This suggests that quercetin glycoside may have stronger and longer-lasting interactions with the receptor, indicating its potential as a potent binder.

ACKNOWLEDGEMENT

I would like to acknowledge the contributions of my Ph.D. supervisory team: Prof. M.I. Sule, Prof. A.M. Musa, Prof. G.O. Adeshina, Prof. B.O. Olayinka, Dr. Ibrahim Atiku, Prof. Asmau Hamza and Prof Sakina Abdullahi

REFRENCES

1. Afolayan, A.J. and Aliero, A.A. (2006) Antimicrobial activity of *Solamnumtomantosum. African Journal of Biotechnology*. 5(4): 369-372.
2. Chiller, K., Selkin, B. A., & Murakawa, G. J. (2001). Skin microflora and bacterial infections of the skin. In *Journal of Investigative dermatology Symposium proceedings* (Vol. 6, No. 3, pp. 170-174). Elsevier
3. Truiti, M. D. C. T., Sarragiotto, M. H., Abreu Filho, B. A. D., Nakamura, C. V. & Dias Filho, B. P. (2003). *In vitro* antibacterial activity of a 7-O-beta-D-glucopyranosyl-nutanocoumarin from *Chaptalia nutans* (Asteraceae). *Memórias do Instituto Oswaldo Cruz*, *98*(2), 283-286.
4. Mahady, G. B., Huang, Y., Doyle, B. J. & Locklear, T. (2008). Natural products as antibacterial agents. *Studies in natural products chemistry*, *35*, 423-444.
5. Górniak, I., Bartoszewski, R. & Króliczewski, J. (2019). Comprehensive review of antimicrobial activities of plant flavonoids. *Phytochemistry Reviews*, *18*(1), 241-272
6. Vaou, N., Stavropoulou, E., Voidarou, C., Tsigalou, C. & Bezirtzoglou, E. (2021). Towards advances in medicinal plant antimicrobial activity: A review study on challenges and future perspectives. *Microorganisms*, *9*(10), 2041.
7. Wabacha, J. K., Gitau, G. K., Bebora, L. C., Bwanga, C. O., Wamuri, Z. M. & Mbithi, P. M. F. (1998). Occurrence of dermatomycosis (ringworm) due to *Trichophyton verrucosumin* dairy calves and its spread to animal attendants: case report. *Journal of the South African Veterinary Association*, *69*(4), 172-173.
8. Swai, E. S. & Sanka, P. N. (2012). Bovine Dermatophytosis caused by *Trichophyton Verrucosum:* a case report. *Vet World*, *5*(5), 297-300.
9. Nowicka, D., Chilicka, K. & Dzieńdziora-Urbińska, I. (2022). Host-Microbe Interaction on the Skin and Its Role in the Pathogenesis and Treatment of Atopic Dermatitis.*Pathogens*, *11*(1), 71.
10. Totté, J. E. E., Van Der Feltz, W. T., Hennekam, M., van Belkum, A., Van Zuuren, E. J., & Pasmans, S. G. M. A. (2016). Prevalence and odds of *Staphylococcus aureus* carriage in atopic dermatitis: a systematic review and meta-analysis. *British Journal of Dermatology*, *175*(4), 687-695.
11. Schrire, B. D., Lavin, M., Barker, N. P., & Forest, F. (2009). Phylogeny of the tribe *Indigofereae* (Leguminosae–Papilionoideae): Geographically structured more in succulent-rich and temperate settings than in grass-rich environments. *American Journal of Botany*, *96*(4), 816-852.
12. Ameen, M. (2010). Epidemiology of superficial

fungal infections. *Clinics in Dermatology*, *28*(2), 197-201.

13. Lademann, J., Patzelt, A., Richter, H., Lademann, O., Baier, G., Breucker, L. & Landfester, K. (2013). Nanocapsules for drug delivery through the skin barrier by tissue-tolerable plasma. *Laser Physics Letters*, *10*(8), 083001
14. Ateba, S. B., Njamen, D., & Krenn, L. (2021). The genus *Eriosema* (Fabaceae): From the ethnopharmacology to an evidence-based phytotherapeutic perspective. *Frontiers in Pharmacology*, *12*, 641225.
15. Timberlake, J. R., Darbyshire, I., Wursten, B., Hadj-Hammou, J., Ballings, P., Mapaura, A., & Shah, T. (2016). Chimanimani Mountains: botany and conservation. *Report produced under CEPF Grant*, *63512*.
16. Darbyshire, I., Kordofani, M., Farag, I., Candiga, R., & Pickering, H. (2015). The plants of Sudan and South Sudan: an annotated checklist.
17. Bonev, B., Hooper, J., & Parisot, J. (2008). Principles of assessing bacterial susceptibility to antibiotics using the agar diffusion method. *Journal of antimicrobial chemotherapy*, *61*(6), 1295-1301.
18. Singh, S., Taneja, B., Salvi, S. S., & Agrawal, A. (2009). Physical properties of intact proteins may predict allergenicity or lack thereof. *PloS one*, *4*(7), e6273.
19. Wang, Z., Zhang, Q., Ding, K., Qin, M., Zhuang, X., Li, X., & Chen, H. (2024). Instruct protein: Aligning human and protein language via knowledge instruction. In *Proceedings of the 62nd Annual Meeting of the Association for Computational Linguistics (Volume 1: Long Papers)* (pp. 1114-1136).
20. Trott, O., & Olson, A. J. (2010). AutoDock Vina: improving the speed and accuracy of docking with a new scoring function, efficient optimization, and multithreading. *Journal of Computational Chemistry*, *31*(2), 455-461.
21. Yang, Z., Lasker, K., Schneidman-Duhovny, D., Webb, B., Huang, C. C., Pettersen, E. F., & Ferrin, T. E. (2012). UCSF Chimera, MODELLER, and IMP: an integrated modeling system. *Journal of structural biology*, *179*(3), 269-278.
22. Sanner, M. F., Olson, A. J., & Spehner, J. C. (1996). Reduced surface: an efficient way to compute molecular surfaces. *Journal of Biopolymers*, *38*(3), 305-320.
23. Syahri, J., Rullah, K., Armunanto, R., Yuanita, E., Nurohmah, B. A., Aluwi, M. F. F. M., & Wai, B. P. (2016). Synthesis, biological evaluation, QSAR analysis, and molecular docking of chalcone derivatives for antimalarial activity. *parasite*, *4*(8), 10-12980.
24. Sani, Y. M., Musa, A. M., Abdullahi, S. M., Nasir, T., Abdullahi, M. I. and Atiku, I. (2015). Quercetin and β-sitosterol isolated from the methanol leaves extract of *Cissuspolyantha* Glig and Brandt (*Vitaceae*). *Nigerian Journal of Pharmaceutical Sciences*. 14(2): 46 -50.
25. Abubakar, H., Musa, A. M., Abdullahi, M. I., Mzozoyana, V., & Yusuf, A. J. (2020). Isolation and characterization of some flavonoids from the leaf of *Tapinanthus globiferus* growing on Vitexdoniana. *Brazilian Journal of Biological Sciences*, *7*(17), 239-245.
26. Bhaskar, B. V., Mohan, A. R., Babu, T. M. C., Rajesh, S. S., Bhuvaneswar, C., Sivaraman, T., & Rajendra, W. (2016). Antibacterial efficacy of fractions and compounds from *Indigofera barberi*: Identification of DNA gyrase B inhibitors through pharmacophore based virtual screening. *Process Biochemistry*, *51*(12), 2208-2221. https://doi.org/10.1016/j.procbio.2016.08.031
27. Sundarrajan, S., & Arumugam, M. (2017). A systems pharmacology perspective to decipher the mechanism of action of Parangichakkaichooranam, a Siddha formulation for the treatment of psoriasis. Journal of *Biomedicine & Pharmacotherapy*, *88*, 74-86.
28. Ahmadu, A. A., Onanuga, A., & Ebeshi, B. U. (2011). Isolation of antibacterial flavonoids from the aerial parts of *Indigofera secundiflora*. *Pharmacognosy Journal*, *3*(19), 25-28.
29. Silva, A. R., Fagundes, C. M. S., Andrade-da-Costa, B. L. S., & Rodrigues, M. C. A. (2014). 071—(SIL0192) Anticonvulsant properties of *Indigofera suffruticosa* in the intra hippocampal pilocarpine model in rats. *Epilepsy & Behavior*, *38*, 212-213.
30. Shahat, A. A., Abdelshafeek, K. A., & Husseiny, H. A. (2011). Isolation and identification of a new flavonoid glycoside from Carrichtera annua L. seeds. *Pharmacognosy Research*, *3*(3), 151.
31. Nunez, H. A., Walker, T. E., Fuentes, R., O'Connor, J., Serianni, A., & Barker, R. (1977). Carbon-13 as a tool for the study of carbohydrate structures, conformations and interactions. *Journal of supramolecular structure*, *6*(4), 535-550.

32. Bubb, W. A. (2003). NMR spectroscopy in the study of carbohydrates: Characterizing the structural complexity. *Concepts in Magnetic Resonance Part A: An Educational Journal*, *19*(1), 1-19.
33. Arung, E. T., Yoshikawa, K., Shimizu, K., & Kondo, R. (2010). Isoprenoid-substituted flavonoids from wood of Artocarpus heterophyllus on B16 melanoma cells: cytotoxicity and structural criteria. *Fitoterapia*, *81*(2), 120-123.
34. Stalikas, C. D. (2007). Extraction, separation, and detection methods for phenolic acids and flavonoids. *Journal of separation science*, *30*(18), 3268-3295.
35. Wang, H., Yang, Y., & Abe, I. (2024). Modifications of prenyl side chains in natural product biosynthesis. *Angewandte Chemie International Edition*, *63*(52), e202415279.
36. Elmi, A., Spina, R., Abdoul-Latif, F., Yagi, S., Fontanay, S., Risler, A. & Laurain-Mattar, D. (2018). Rapid screening for bioactive natural compounds in *Indigofera caerulea* Roxfruits. *Industrial Crops and Products*, *125*, 123-130
37. Samuelsson, G., Farah, M. H., Claeson, P., Hagos, M., Thulin, M., Hedberg, O. & Alin, M. H. (1992). Inventory of plants used in traditional medicine in Somalia. II. Plants of the families Combretaceae to Labiatae. *Journal of Ethnopharmacology*, *37*(1), 47-70.
38. De Montellano, B. R. O., & Browner, C. H. (1985). Chemical bases for medicinal plant use in Oaxaca, Mexico. *Journal of ethnopharmacology*, *13*(1), 57-88.
39. Campos, J. K., Araujo, T. F. D. S., Brito, T. G. D. S., da Silva, A. P., Cunha, R. X. D., Martins, M. B., & Lima, V. L. D. M. (2018). *Indigofera suffruticosa* Mill. (Anil): Plant profile, phytochemistry, and pharmacology review. *Advances in Pharmacological and Pharmaceutical Sciences*, *2018*.
40. Dennis, E. A., Cao, J., Hsu, Y. H., Magrioti, V., & Kokotos, G. (2011). Phospholipase A2 enzymes: Physical structure, biological function, disease implication, chemical inhibition, and therapeutic intervention. *Chemical Reviews, 111*(10), 6130–6185.
41. Bissantz, C., Kuhn, B., & Stahl, M. (2010). A medicinal chemist's guide to molecular interactions. *Journal of Medicinal Chemistry, 53*(14), 5061–5084.
42. Burke, J. E., & Dennis, E. A. (2009). Phospholipase A2 structure/function, mechanism, and signaling. *Journal of Lipid Research, 50*(Supplement), S237–S242.
43. Ferreira, L. G., dos Santos, R. N., Oliva, G., & Andricopulo, A. D. (2015). Molecular docking and structure-based drug design strategies. *Search forMolecules, 20*(7), 13384–13421.
44. Salonen, L. M., Ellermann, M., & Diederich, F. (2011). Aromatic rings in chemical and biological recognition: Energetics and structures. *Angewandte Chemie International Edition, 50*(21), 4808–4842.
45. Panula, P., Chazot, P. L., Cowart, M., Gutzmer, R., Leurs, R., Liu, W. L., Stark, H., Thurmond, R. L., & Haas, H. L. (2015). International Union of Basic and Clinical Pharmacology. XCVIII. Histamine receptors. *Pharmacological Reviews, 67*(3), 601–655.
46. Venkatakrishnan, A. J., Deupi, X., Lebon, G., Heydenreich, F. M., Flock, T., Miljus, T., Balaji, S., Bouvier, M., Veprintsev, D. B., Tate, C. G., Schertler, G. F. X., & Babu, M. M. (2016). Diverse activation pathways in class A GPCRs converge near the G-protein-coupling region. *Nature, 536*(7617), 484–487
47. Gerometta, E., Grondin, I., Smadja, J., Frederich, M., & Gauvin-Bialecki, A. (2020). A review of traditional uses, phytochemistry and pharmacology of the genus Indigofera. *Journal of ethnopharmacology*, *253*, 112608.
48. Kufareva, I., Katritch, V., Stevens, R. C., & Abagyan, R. (2014). Advances in GPCR modeling evaluated by the GPCR Dock 2013 assessment: meeting new challenges. *Structure*, *22*(8), 1120-1139.